Journal of Hydrology 530 (2015) 167–179

Contents lists available at ScienceDirect

Journal of Hydrology

journal homepage: www.elsevier.com/locate/jhydrol

High-resolution prediction of soil available water content within the crop root zone

Amir Haghverdi [a,b,*], Brian G. Leib [b], Robert A. Washington-Allen [c], Paul D. Ayers [b], Michael J. Buschermohle [c]

[a] Department of Biological Systems Engineering, University of Nebraska-Lincoln, Panhandle Research and Extension Center, 4502 Avenue I, Scottsbluff, NE 69361-4939, United States
[b] Department of Biosystems Engineering & Soil Science, University of Tennessee, 2506 E.J. Chapman Drive, Knoxville, TN 37996-4531, United States
[c] Department of Geography, University of Tennessee, Burchfiel Geography Building, 1000 Phillip Fulmer Way, Knoxville, TN 37996-0925, United States

ARTICLE INFO

Article history:
Received 6 June 2015
Received in revised form 19 September 2015
Accepted 22 September 2015
Available online 1 October 2015
This manuscript was handled by Andras Bardossy, Editor-in-Chief, with the assistance of J.A. Huisman, Associate Editor

Keywords:
Apparent electrical conductivity (EC_a)
Available water content (AWC)
Pedotransfer function (PTF)
Water retention curve (WRC)

SUMMARY

A detailed understanding of soil hydraulic properties, particularly soil available water content (AWC) within the effective root zone, is needed to optimally schedule irrigation in fields with substantial spatial heterogeneity. However, it is difficult and time consuming to directly measure soil hydraulic properties. Therefore, easily collected and measured soil properties, such as soil texture and/or bulk density, that are well correlated with hydraulic properties are used as proxies to develop pedotransfer functions (PTF). In this study, multiple modeling scenarios were developed and evaluated to indirectly predict high resolution AWC maps within the effective root zone. The modeling techniques included kriging, co-kriging, regression kriging, artificial neural networks (NN) and geographically weighted regression (GWR). The efficiency of soil apparent electrical conductivity (EC_a) as proximal data in the modeling process was assessed. There was a good agreement (root mean square error (RMSE) = 0.052 $cm^3\ cm^{-3}$ and $r = 0.88$) between observed and point prediction of water contents using pseudo continuous PTFs. We found that both GWR (mean RMSE = 0.062 $cm^3\ cm^{-3}$) and regression kriging (mean RMSE = 0.063 $cm^3\ cm^{-3}$) produced the best water content maps with these accuracies improved up to 19% when EC_a was used as an ancillary soil attribute in the interpolation process. The maps indicated fourfold differences in AWC between coarse- and fine-textured soils across the study site. This provided a template for future investigations for evaluating the efficiency of variable rate irrigation management scenarios in accounting for the spatial heterogeneity of soil hydraulic attributes.

1. Introduction

Across the globe, water has become the most valuable input for agriculture. The growing demand for food and fiber production along with uncertainties in rainfall patterns has resulted in increased attention on irrigation practices. If field-level spatial soil variation is substantial, variable rate irrigation becomes a desirable method to apply an optimum amount of water to each soil type in order to maximize yield. Duncan (2012) conducted a two-year cotton irrigation study and showed that the optimum supplemental irrigation strategy was different among plots with high, moderate and low water holding capacity (WHC). He emphasized that in the long term it is not possible to maximize yield with a uniform supplemental irrigation strategy in fields with a significant degree of heterogeneity in soil available water content (AWC).

Soil hydraulic information is required for the majority of agro-hydrological studies and irrigation management including providing essential inputs for irrigation, drainage, and hydrological models. The main goal of these endeavors is to account for the spatial heterogeneity of these hydraulic properties by mapping their spatial distribution at high resolution. However, obtaining information on soil hydraulic properties such as soil water retention and hydraulic conductivity is challenging due to the time-consuming and labor-intensive nature of *in situ* and laboratory methods. The traditional solution to this problem was to develop proxies of soil hydraulic properties by collecting easily measured soil characteristics such as texture, bulk density, and organic matter content that are well correlated with soil hydraulic properties

* Corresponding author at: Department of Biological Systems Engineering, University of Nebraska-Lincoln, Panhandle Research and Extension Center, 4502 Avenue I, Scottsbluff, NE 69361-4939, United States. Tel.: +1 (308) 632 1246 (office).
E-mail address: ahaghverdi2@unl.edu (A. Haghverdi).

http://dx.doi.org/10.1016/j.jhydrol.2015.09.061
0022-1694/

to produce pedotransfer functions (PTFs, Bouma, 1989). Another easily collected soil attribute is apparent electrical conductivity (EC_a), which is a function of the electrical conductivity of porous media solution, the soil porosity, and the cementation exponent, i.e., Archie's law (Archie, 1942). When soil salinity is not a major factor, EC_a may be a useful proxy of soil physical and hydraulic attributes (Sudduth et al., 2005) including depth to sand layer (Duncan, 2012), clay percentage under non-saline conditions (Saey et al., 2009), and soil texture and WHC (Abdu et al., 2008). Abdu et al. (2008) predicted WHC in the subsurface soil of a small watershed using EC_a data. Their PTFs for clay percentage ($r = 0.86$) and WHC ($r = 0.75$) showed good performance, but they emphasized the need for additional studies to appropriately relate EC_a to other soil hydraulic attributes, a goal of this particular study (Abdu et al., 2008).

PTFs were initially derived using multiple regression techniques, but machine-learning algorithms are now predominantly used to derive PTFs (Vereecken et al., 2010). A combination of PTFs and interpolation techniques is usually required to generate a map of soil hydraulic properties. For example, Ferrer Julià et al. (2004) used kriging to interpolate the PTF of saturated hydraulic conductivity to produce a 1-km^2 resolution saturated hydraulic conductivity map of Spain. They reported that soil texture was the most important input predictor to the PTF, while organic matter content showed a low influence on saturated soils (Ferrer Julià et al., 2004). In recent years, alternative interpolation techniques have been introduced and evaluated to map the spatial variability of environmental attributes such as regression kriging, geographically weighted regression (GWR), and machine learning-based spatial models (Eldeiry and Garcia, 2010; Li et al., 2011; Sharma et al., 2011). Herbst et al. (2006) compared the use of different interpolation techniques in conjunction with terrain attributes such as slope to predict soil hydraulic properties in a micro-scale catchment. They found that regression kriging had the smallest average prediction error and thus was the most appropriate method to use. Additionally, they found up to 15% improvement in spatial predictions of hydraulic properties when using terrain attributes as co-variables in comparison with ordinary kriging without co-variables.

Traditionally, two modeling approaches, the CI and the IC, have been implemented to produce maps of predicted soil physical and hydraulic properties. One can first run PTFs at individual points or locations of input variables throughout the area of interest and then interpolate the point predictions to generate maps, i.e. using a 'calculate first, interpolate later' (CI) approach. Alternatively, one can interpolate the soil attribute, such as bulk density, texture or organic matter content across the study area and then convert the soil attribute maps to soil hydraulic properties maps by PTFs, i.e.; an 'interpolate first, calculate later' (IC) approach. Many researchers have compared different IC procedures against CI techniques (e.g. Sinowski et al., 1997; Heuvelink and Pebesma, 1999; Bechini et al., 2003), yet the reported results are different and do not indicate the supremacy of either procedure. However, procedures to predict the spatial distribution of soil hydraulic properties may be improved with the additional use of on-the-go sensing (e.g. Hedley and Yule, 2009a, 2009b; Hedley et al., 2013) and remote sensing (e.g. Jana and Mohanty, 2011) technologies.

Consequently, the objectives of this study are to

(i) Develop PTFs from soil physical properties within the effective crop root zone.
(ii) Determine the best interpolation method for generating AWC maps at the field spatial scale.
(iii) Investigate the use of EC_a to improve spatial prediction of AWC.

2. Materials and methods

2.1. Study area & collection of soil physical/hydraulic data

The 73 ha field of study is located in west Tennessee close to the Mississippi River (Fig. 1). The field contained two center pivot irrigation systems that were used for supplemental irrigation of no-till cotton during each cropping season. Field soil sampling was conducted from March 20 to 22, 2014 after rainfall events when soil was assumed to be close to field capacity. A truck mounted hydraulic probe was used on March 21 and 22, 2014 to sample 100 undisturbed sites at 0–100 cm depth (Fig. 1). Fig. 1 shows the sampling scheme where each soil sample was divided into four segments. Hereafter, the word "layer" is used to distinguish among subsamples rather than real soil horizons. The default depth of subsamples was 25-cm, though adjustments were made that accounted for soil horizon transitions. Soil texture, bulk density (BD), and gravimetric water content were measured in the lab. Prior to this, on March 20, 2014, EC_a was measured at 4700 points at shallow (0–30-cm) and deep (0–90-cm) depths across the study area using a Veris 3100 (Veris Technologies, Salina, KS).

The Veris 3100 uses the principle of electrical resistivity to measure EC_a. A small electrical current is introduced by a pair of coulter-electrodes (rotating disks) into the soil and the drop in voltage at two different depths [i.e., shallow (approximately 0–30 cm) and deep (approximately 0–90 cm)] are measured (Sudduth et al., 2005). The current flowing through three different conductance pathways (i.e. liquid, soil-liquid and solid) affects the measure of EC_a (Corwin and Lesch, 2005; Sudduth et al., 2005). In this study, the shallow EC_a readings exhibited a normal distribution, but the deep EC_a readings were skewed and thus needed to be log transformed.

2.2. Pedotransfer function development

To predict soil water retention curves (WRCs), i.e., the relationship between water content and soil matric potential, for the

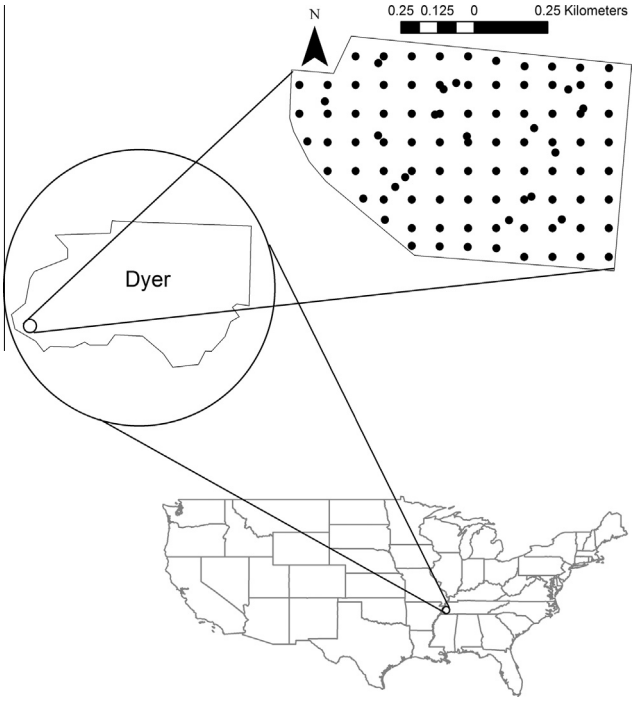

Fig. 1. The soil sampling scheme of soil physical properties that was used within a 73-ha study field of cotton that is located in Dyer County, Tennessee.

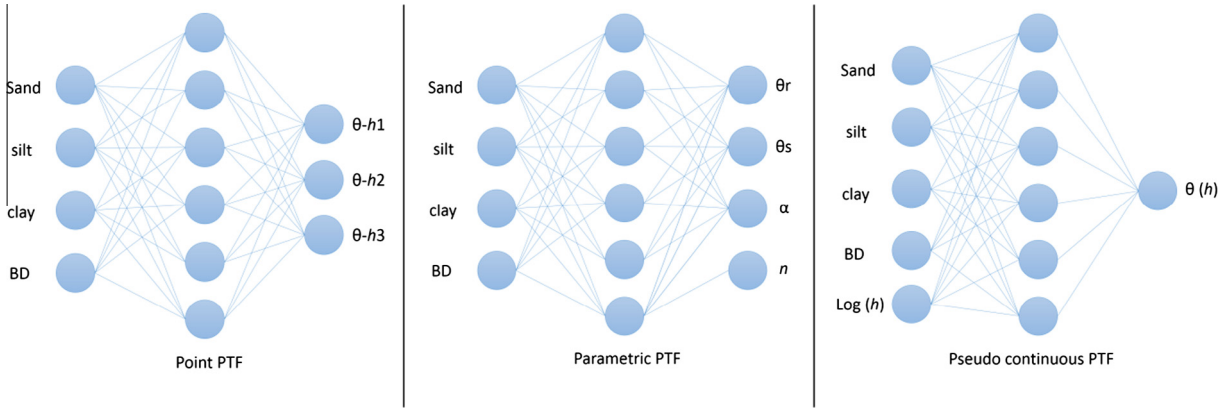

Fig. 2. The topologies of point, parametric, and pseudo continuous neural network (PC) pedotransfer functions (PTFs) are compared to each other. Haghverdi et al. (2012) developed the PC-PTF. The point and parametric PTFs use soil texture and bulk density to predict water content at three different matric potentials (i.e., $h1$, $h2$ and $h3$) and four different inputs to the van Genuchten equation (van Genuchten, 1980), respectively. The PC-PTF uses these 2 soil properties and soil matric potential [Log (h)] to predict the water content.

collected soil samples, a pseudo continuous PTF (PC-PTF) was developed (Fig. 2). Haghverdi et al. (2012) first introduced the concept of PC-PTF as an alternative approach to point (Type 2) and parametric (Type 3) PTFs (nomenclature from Wösten et al., 2001). Point PTFs only predict water retention at a limited amount of water retention points. Parametric PTFs predict parameters of input to a soil hydraulic equation [e.g., the van Genuchten model (Van Genuchten, 1980)] that is used to predict the WRC (Fig. 2). A PC-PTF relies on the power of machine learning algorithms to predict the WRC using a limited amount of measured water retention points (Haghverdi et al., 2014). The developed PC-PTF uses sampled soil texture and BD from the field as well as the logarithm of the soil matric potential [e.g. Log (15,296 cm H_2O) = 4.18] as input parameters to predict water content (Fig. 2). With the input of a wide range of soil matric potentials a corresponding range of water contents can be predicted that results in the generation of a pseudo-continuous WRC (Haghverdi et al., 2014).

A subset (n = 554) of the Unsaturated Soil Hydraulic Database (UNSODA) (Nemes et al., 2001) was selected to establish PC-PTFs. The UNSODA contains a variety of information on soil hydraulic properties including WRCs and hydraulic conductivity, as well as soil properties that include particle-size distribution, BD and organic matter content. To derive a reliable PC-PTF, it is essential to have soils that are similar in their basic properties in the training and prediction data sets. Table 1 and Fig. 3 compare the descriptive statistics and the distribution of soil texture for the soil samples collected in the field and the selected UNSODA samples. We found that the samples from UNSODA are representative of the range of coarse textures in the texture triangle and thus are similar to the sampled soils from the study area.

The PC-PTF was derived using a three layer feed forward back propagation neural network (NN) with sigmoid tangent hyperbolic and linear activation functions in hidden and output layers, respectively (Haghverdi et al., 2012, 2014). The Levenberg–Marquardt algorithm (Demuth and Beale, 2000) was used to train the NN. The UNSODA samples were divided into 10 almost equal subsets and each subset was once assigned to the model validation phase, while the other 9 subsets were used for *development* of the PTFs. The number of neurons in the hidden layer was changed from 1 to 20 when a cross-validation procedure was performed to identify the best structure. A sampling with replacement technique (Efron and Tibshirani, 1993) was applied on the *development* data to create 50 statistically similar subsets of the same size for training. It was expected that each subset had about 63% of the parent dataset (Schaap et al., 2001). The rest of the samples, i.e. 37% of the parent dataset, were assigned to the cross-validation procedure. The training process was terminated when an increase in prediction error was observed for the cross-validation dataset. A bootstrap aggregating technique was used to yield the mean PTF prediction where a submodel was established on each subset and the predictions by the submodels were averaged. The Matlab R2014a environment (MathWorks, Inc., Natick, Mass.) was used to develop these models. Once the PC-PTF was derived, a continuous prediction of water retention over a wide range of matric potentials was obtained.

Table 1
The physical soil characteristics including bulk density (BD) and soil texture selected from the Unsaturated Soil Hydraulic Database (UNSODA) and collected from the study site to predict soil hydraulic properties.

	UNSODA (n = 554)				The field (n = 400)			
	Min	Max	SD	Average	Min	Max	SD	Average
Sand (%)	0.1	99.6	31.2	53.8	0.0	96.9	30.2	53.9
Silt (%)	0.2	87.1	22.9	29.7	0.0	72.8	19.7	27.3
Clay (%)	0.0	63.0	13.6	16.6	0.3	56.6	12.7	18.8
BD (Mg m^{-3})	0.46	1.97	0.22	1.46	1.06	1.86	0.12	1.36

BD: bulk density, SD: standard deviation.

2.3. Spatial modeling of AWC

AWC is obtained as the difference between water content at field capacity (FC) and permanent wilting point (PWP). The FC and PWP are widely used thresholds for irrigation management. FC is a qualitative parameter that is a practical and understandable indicator of soil WHC (Romano and Santini, 2002). Water retentions at −10 and −33 kPa could be considered as FC for coarse- and fine-textured soils, respectively (Rivers and Shipp, 1972). The water content at −1500 kPa is usually chosen as the PWP for all soil textures. For this study, we assumed that at FC, matric potential was uniform across the study area (−10 kPa). However, 3 high-resolution maps were predicted for water content at −10, −33 and −1500 kPa across the study site providing the opportunity to consider two matric potentials for water content at FC in further studies if needed.

Ten spatial modeling scenarios that used kriging, co-kriging, regression kriging, GWR and NNs were examined (Fig. 4). The objective was to convert soil properties at point locations to continuous maps of soil properties and to evaluate the efficiency of the EC_a as a proximal attribute in this process. To evaluate the performance of the models, a cross-validation procedure was

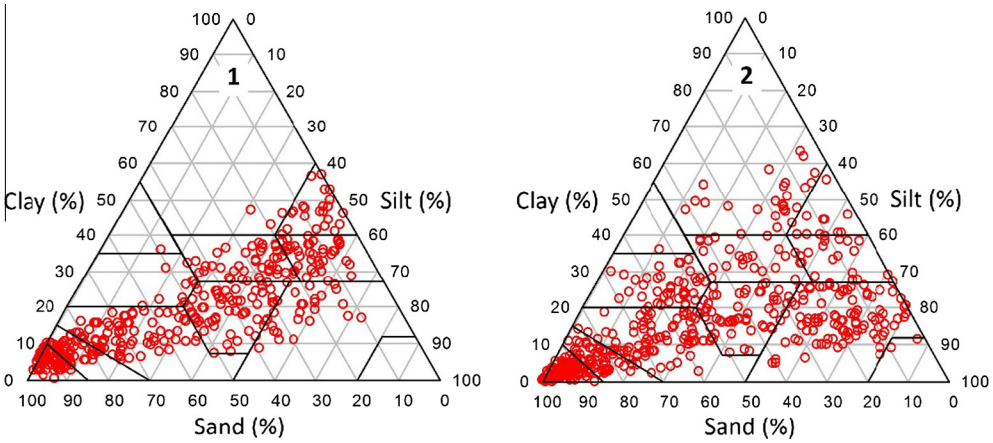

Fig. 3. The distribution of soil texture in samples from the field of study (Texture Triangle 1) and selected samples from the Unsaturated Soil Hydraulic Database (UNSODA, Texture Triangle 2).

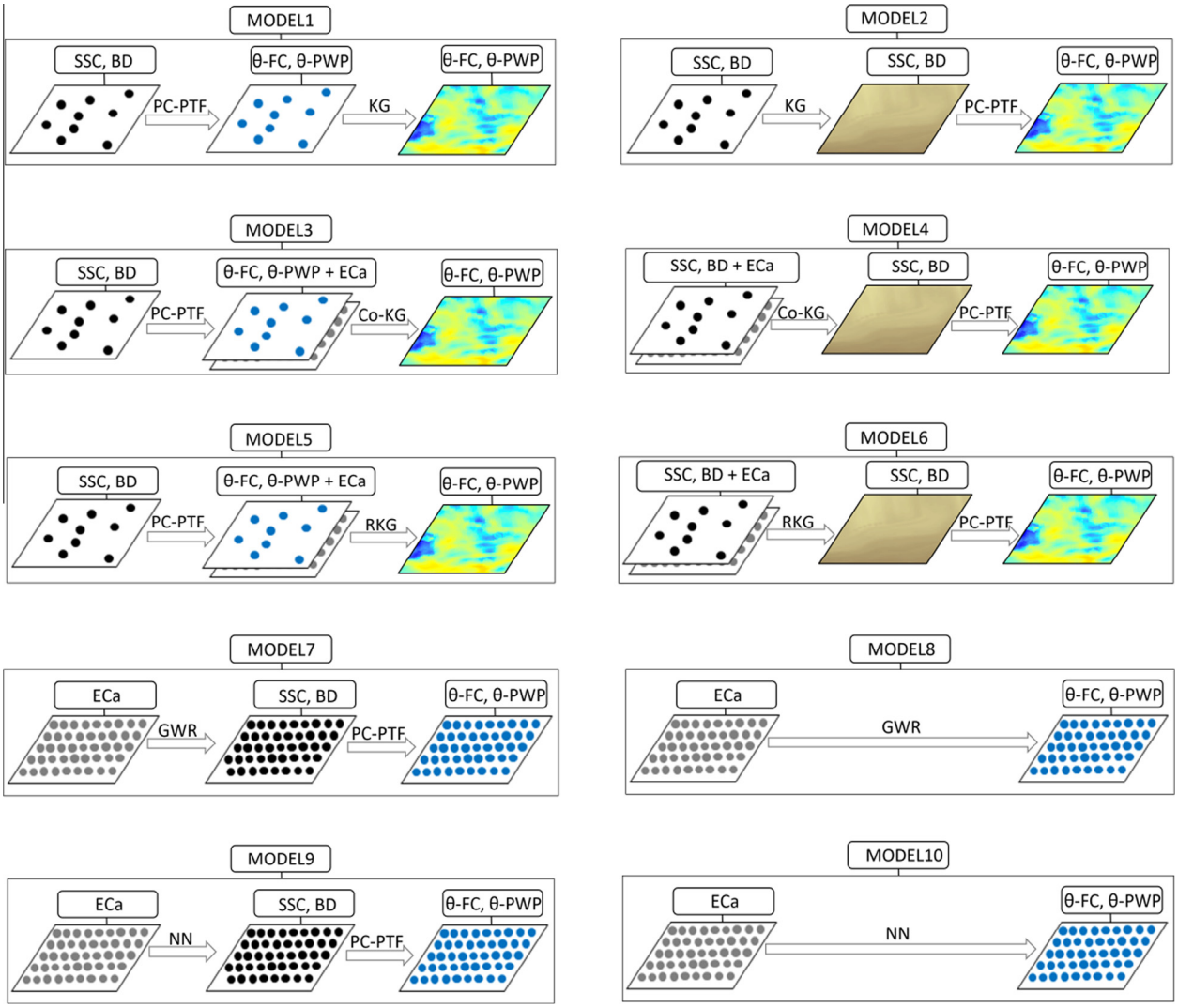

Fig. 4. Ten workflow models were developed and compared to predict water content maps at field capacity (FC, $cm^3\ cm^{-3}$) and permanent wilting point (PWP, $cm^3\ cm^{-3}$). The models used pseudo continuous pedotransfer function (PC-PTF), kriging (KG), co-kriging (Co-KG), regression kriging (RKG), geographically weighted regression (GWR), and/or an artificial neural network (NN). Soil physical variables that were used as water content proxies included soil texture, represented as the percentage of sand, silt and clay (SSC), bulk density (BD, $Mg\ m^{-3}$), and apparent electrical conductivity (EC_a, $mS\ m^{-1}$).

designed. First, soil samples were randomly divided into 5 groups (the groups were identical among soil layers). AWC maps were then derived using 4 groups out of five. The fifth group was used to validate the performance of the models. This task was repeated 5 times in order to involve all the samples in the cross-validation process.

2.3.1. Kriging, co-kriging and regression kriging

Ordinary kriging, co-kriging and regression kriging were used in the models 1–6 (Fig. 4). ArcGIS 10.2.2 (ESRI Inc., Redlands, California) and RStudio 0.98.1103 (RStudio, Inc., Boston, Ma, USA) were used to derive these models. Model 1 and Model 2 used PC-PTF for calculation and kriging to interpolate. Co-kriging was used instead of kriging in models 3 and 4 where shallow and deep EC_a were considered as the proximal attributes for layers one and two/three/four, respectively. Regression kriging was used in models 5 and 6. Kriging is an interpolation procedure that assumes that unknown locations of attributes of interest are spatially autocorrelated and normally distributed from sampled locations thus accounting for the distance, direction, and the overall spatial arrangement between known and unknown points (Oliver, 2010). Additionally, kriging includes an evaluation of the prediction uncertainty (Oliver, 2010). Cokriging is an extension of the kriging technique that uses ancillary information, such as elevation or other topographic variables to predict the spatial distribution of main variables of interest (Goovaerts and Kerry, 2010). Cokriging uses both the semivariogram of the main attribute and the cross-semivariogram of the proximal or ancillary attribute(s) to improve predictions (Goovaerts and Kerry, 2010). The semivariogram and cross-semivariogram are estimated as follows:

$$\gamma_{uv}(\mathbf{h}) = \frac{1}{2N(\mathbf{h})}\sum_{i=1}^{N(\mathbf{h})}\{[Z_u(\mathbf{x_i}+\mathbf{h}) - Z_u(\mathbf{x_i})][Z_v(\mathbf{x_i}+\mathbf{h}) - Z_v(\mathbf{x_i})]\} \quad (1)$$

where γ_{uv} is the cross-semivariance when $u \neq v$ and is the semivariance when $u = v$; u is the main attribute; v is the proximal attribute; $\mathbf{h}$ is the interval class; $N(\mathbf{h})$ is the number of pairs separated by lag distance; and $Z(\mathbf{x_i})$ and $Z(\mathbf{x_i}+\mathbf{h})$ are measured attributes at spatial locations i and $i+\mathbf{h}$, respectively. The general form of kriging (Eq. (2)) and cokriging (Eq. (3)) estimators are as follows:

$$Z^*(\mathbf{x_p}) = \sum_{i=1}^{I}\lambda_i Z(\mathbf{x_i}) \quad (2)$$

where $Z^*(\mathbf{x_p})$ is the prediction at the target location $\mathbf{x_p}$; λ_i and $Z(\mathbf{x_i})$ are weight of the attribute and the attribute value at ith location, respectively; and I is the number of measured values.

$$Z^*(\mathbf{x_p}) = \sum_{i=1}^{I}\lambda_i Z(\mathbf{x_i}) + \sum_{j=1}^{J}\lambda_j Z(\mathbf{x_j}) \qquad \mathbf{s.t.}\sum_{i=1}^{I}\lambda_i = 1; \sum_{i=1}^{J}\lambda_j = 0 \quad (3)$$

where the main and proximal attributes are indicated by i and j, respectively, and J is the number of measured values for the proximal attribute; and the other parameters are as previously defined.

Regression kriging is a hybrid interpolation technique that initiates with a regression on the proximal data and then uses kriging to interpolate the regression's residuals as follows (Hengl et al., 2007):

$$Z^*(\mathbf{x_p}) = \hat{\beta}_0 + \sum_{k=0}^{n}\hat{\beta}_k \cdot q_k(\mathbf{x_P}) + \sum_{i=1}^{m}\lambda_i . e(\mathbf{x_i}) \quad (4)$$

where $\hat{\beta}_0$ is the estimated intercept, $\hat{\beta}_k$ is coefficient for the kth variable of the regression model (drift model) and $q_k(\mathbf{x_P})$ is the value of proximal attribute at location $\mathbf{x_P}$, n is the number of proximal attributes, λ_i and $e(\mathbf{x_i})$ are the weight of a residual and the residual's value at location $\mathbf{x_i}$, respectively. The m is the number of measured values.

The 'calculate first, interpolate later' (CI) approach was used in models 1, 3 and 5 and the 'interpolate first, calculate later' (IC) approach was used in models 2, 4 and 6 (Fig. 4). If an attribute showed a non-Gaussian distribution, then the data were transformed to approximate a normal distribution. Empirical semivariograms were calculated using the Geostatistical Analyst toolbox in ArcGIS 10.2.2 (ESRI Inc., Redlands, California) considering 12 lags and an omnidirectional stable model.

2.3.2. Geographically weighted regression

For models 7 and 8 we used a geographically weighted regression (GWR), a spatial regression technique that models local or neighborhood relationships between variables and responses, thus accounting for the influence of spatial autocorrelation on standard regressions (Fotheringham et al., 2002). This statistical method defines a bandwidth for each data point and produces a regression equation using the data that falls within the bandwidth (Fotheringham et al., 2002). The coefficients in GWR form a continuous surface representing the spatial variation:

$$Z^*(\mathbf{x_p}) = \hat{\beta}_0(\mathbf{x_p}) + \sum_k \hat{\beta}_k(\mathbf{x_p}) \times \mathbf{x}_k(\mathbf{x_p}) + \varepsilon(\mathbf{x_p}) \quad (5)$$

where $\hat{\beta}_0$ is the intercept and $\hat{\beta}_k$ is the coefficient for the kth variable; ε is the error associated with the point P; and the other parameters are as previously defined.

In model 7, the GWR was used to predict the characteristics of soil texture and BD that were subsequently used as input predictors to produce an estimate of water retention at FC and a PWP using PC-PTF. In model 8, the GWR was used to directly predict water retention at FC and PWP. Both shallow and deep (log transformed) EC_a readings were considered as input predictors for all soil layers. To perform each local regression analysis, the optimum distance (fixed kernel) was automatically obtained using the Akaike Information Criterion (AIC). Models 7 and 8 were derived using GWR in ArcGIS 10.2.2 (ESRI Inc., Redlands, California).

2.3.3. Artificial neural network

The workflows for models 9 and 10 are similar to models 7 and 8, except rather than GWR, NN was used. Both shallow and deep (log transformed) EC_a readings were considered as input predictors for all soil layers. The coordinates of samples were considered as extra input predictors, enabling the NN to learn the dependency of the sampling locations hence working as a spatial model. SPSS Modeler 15 (SPSS Inc., Chicago, IL, USA) was used to derive models. The best number of neurons in the hidden layer was automatically computed. The bootstrap aggregating technique was implemented to enhance model stability and the number of ensembles was equal to 50. Thirty percent of the training data were assigned to cross-validation to avoid over-fitting.

2.4. Yield data collection

The correlation between AWC throughout the effective root zone, EC_a data, and crop yield was determined. Two available yield data sets (collected and stored by the farmer using the appropriate yield monitors) were selected: soybean from 2009 and cotton from 2012. Presently, the majority of the field is covered by two center pivots. The rainfall is usually high during the cropping season, yet the farmer practices uniform supplemental irrigation whenever unpredicted dry periods occur. The raw yield data were pre-processed to remove outliers and bad data. The data greater/smaller than 3 times the standard deviation from the mean were assumed to be statistically unexpected and removed unless there was scientific evidence acting against this assumption (e.g. very low yield on rain-fed areas in a dry year). After removing outliers

approximately 27,000–54,000 yield data points were retained in soybean and cotton maps, respectively. To calculate the correlation, the cleaned yield data first were converted to maps by the ordinary kriging method (25 m^2 cells). Then, the expected yield values at the sampling locations were obtained. The same procedure was implemented to calculated EC_a data at sampling locations.

2.5. Performance evaluation

The performance of the 10 models was evaluated using three statistics: the root mean square error (RMSE), the mean bias error (MBE), and the correlation coefficient (r):

$$\mathrm{RMSE} = \left(\frac{1}{n}\sum_{i=1}^{n}(E_i - M_i)^2\right)^{0.5} \quad (6)$$

$$\mathrm{MBE} = \frac{1}{n}\sum_{i=1}^{n}(E_i - M_i) \quad (7)$$

$$r = \frac{\sum_{i=1}^{n}(M_i - M_m)(E_i - E_m)}{\left(\sum_{i=1}^{n}(M_i - M_m)^2\sum_{i=1}^{n}(E_i - E_m)^2\right)^{0.5}} \quad (8)$$

where E_i, and M_i are the predicted (i.e. the output of the spatial modeling process) and the actual water content (i.e. the outputs of the PC-PTF prior to performing the spatial modeling process) for the ith observation ($cm^3\ cm^{-3}$), respectively; n is the number of actual water content points in test/validation set; E_m and M_m are the mean of predicted and the mean of actual water content ($cm^3\ cm^{-3}$), respectively.

3. Results

3.1. PTF

Fig. 5 shows how the PC-PTF performed in predicting water retention of the UNSODA data set. At first the error sharply decreased as more neurons were added to the hidden layer, but leveled off after about 7–10 neurons. The model with 17 neurons in the hidden layer had the minimum RMSE (0.056 $cm^3\ cm^{-3}$), so was selected for the prediction. Fig. 6 illustrates the WRCs predicted for the collected samples ($n = 400$) from the field of study. The shape of the curves followed the expected pattern: a steep slope at low and intermediate absolute matric potentials for more coarse-textured soils, as opposed to a constant decrease over a wider range of matric potentials for more fine-textured soils.

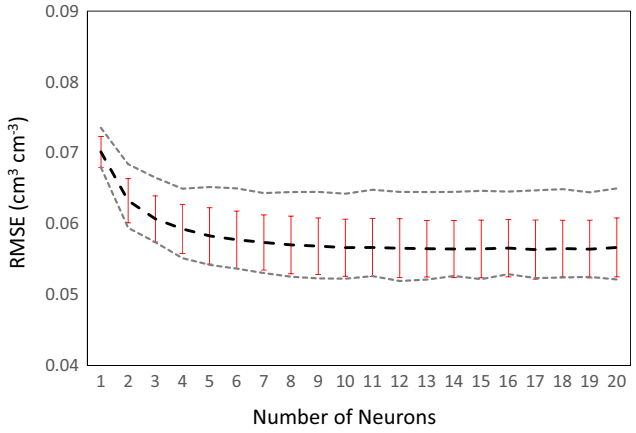

Fig. 5. Performance of the pseudo-continuous neural network pedotransfer functions (PC-PTF) in predicting the water retention curve of samples from the Unsaturated Soil Hydraulic Database (UNSODA). The thick dash line is the mean root mean square error (RMSE), the thin dash lines are the minimum and maximum RMSE, and the error bars are the standard deviation of RMSE values over the 10 subsets.

The study site was close to field capacity during sampling. We took advantage of this status to evaluate the performance of PC-PTF against measured soil water content data from the field of study. The water retention at matric potentials −10 kPa and −33 kPa was predicted and plotted against volumetric water content at the time of sampling (Fig. 7). The points were color coded to distinguish among soil layers where darker circles correspond to samples from deeper layers. There was a very good agreement among predicted and observed water contents with a correlation coefficient (RMSE) equal to 0.87 (0.051 $cm^3\ cm^{-3}$) and 0.88 (0.052 $cm^3\ cm^{-3}$) at −10 kPa and −33 kPa, respectively. MBE were equal to 0.046 $cm^3\ cm^{-3}$ and −0.007 $cm^3\ cm^{-3}$ at −10 kPa and −33 kPa indicating a slight overestimation at −10 kPa. There were soils with low and high WHC at each layer. A cloud of dark circles at low water content, i.e. from 10% to 20%, corresponds well to the presence of some sandy spots across the field of study. There was only one point with volumetric water content more than 60% which was located very close to drainage path. The surface of the drainage path was still wet at the time of sampling, so at a higher water content than the FC.

3.2. Spatial prediction of AWC

Up to now, the WRCs were predicted using PC-PTF for the collected soil samples. Fig. 8 depicts the spatial structure of the water content at FC and PWP along with AWC for different layers. The resulting semivariograms indicated mostly moderate to strong spatial structures. This strong soil spatial variability has likely been created by depositional events, river flood-induced sand boils and/or earthquake-induced sand blows. The average *range* varied from 250 m to 279 m among layers, 2–3 times greater than sampling intervals. This shows the presence of spatial structure beyond sampling distance. With regard to FC, in general, the value for the range decreased with depth. This trend was reversed, however, with regard to the PWP while the subsurface layer (25–50 cm) had the highest range. The *nugget* to *sill* ratio varied from 23% to 60% for water retention data at FC and PWP, except for the water content at the PWP for the first layer which was 0. This could be an artifact of the variogram fitting and calculation since the PWP of the first layer only showed a weak spatial structure. On average, the subsurface layer (i.e. 25–50 cm) had the highest nugget to sill ratio. The AWC data exhibited some randomness and inconsistency in their spatial structure for the first and second layers. Therefore, AWC maps were produced for individual layers by subtracting interpolated FC maps (i.e. −10 kPa) from PWP maps.

Tables 2 and 3 summarize performance of the models for each individual soil layer in terms of RMSE and MBE, respectively. The model 1, 3 and 5 almost always had a better performance and lower bias than model 2, 4 and 6, respectively. Therefore, applying PC-PTF to predict water retention on discrete sampling locations and subsequently interpolating those predictions to generate a map is suggested (i.e. CI). Co-kriging using EC_a as ancillary attribute enhanced the accuracy of interpolation in comparison with ordinary kriging for both CI (i.e. 17% lower mean RMSE for model 3 comparing to model 1) and IC (i.e. 8% lower mean RMSE for model 4 comparing to model 2) approaches. The regression kriging showed higher accuracy (19% lower mean RMSE) than ordinary-kriging for CI approach (model 5 versus model 1) for all layers and matric potentials except for water content predictions at −1500 kPa for the deep layer, but this improvement was not consistent for the IC approach across layers and matric potentials. In

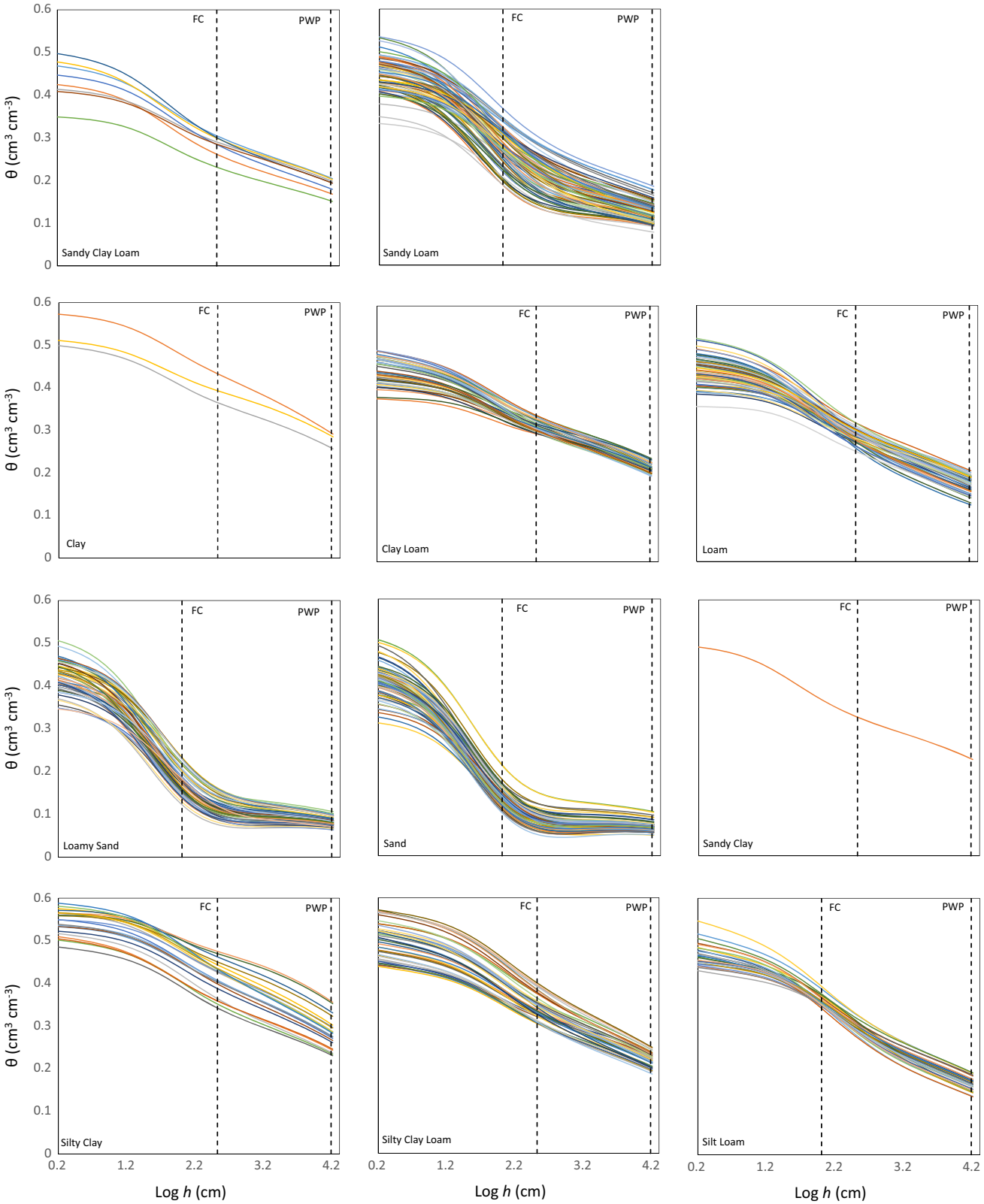

Fig. 6. The predicted water retention curves at different soil textures that were derived using the pseudo-continuous pedotransfer function (PC-PTF) for the soil samples (n = 400) collected from the study site in west Tennessee. The water contents predicted at field capacity (FC) and permanent wilting point (PWP) are then used to calculate soil AWC.

11 out of 12 cases, GWR based models worked more accurately than NN based models but the differences were minor such that average RMSE for models 7, 8, 9 and 10 were 0.063 $cm^3\ cm^{-3}$, 0.062 $cm^3\ cm^{-3}$, 0.064 $cm^3\ cm^{-3}$ and 0.066 $cm^3\ cm^{-3}$, respectively. There is no best model for all the matric potentials and layers. Overall, models 8 (RMSE = 0.062 $cm^3\ cm^{-3}$) following by models

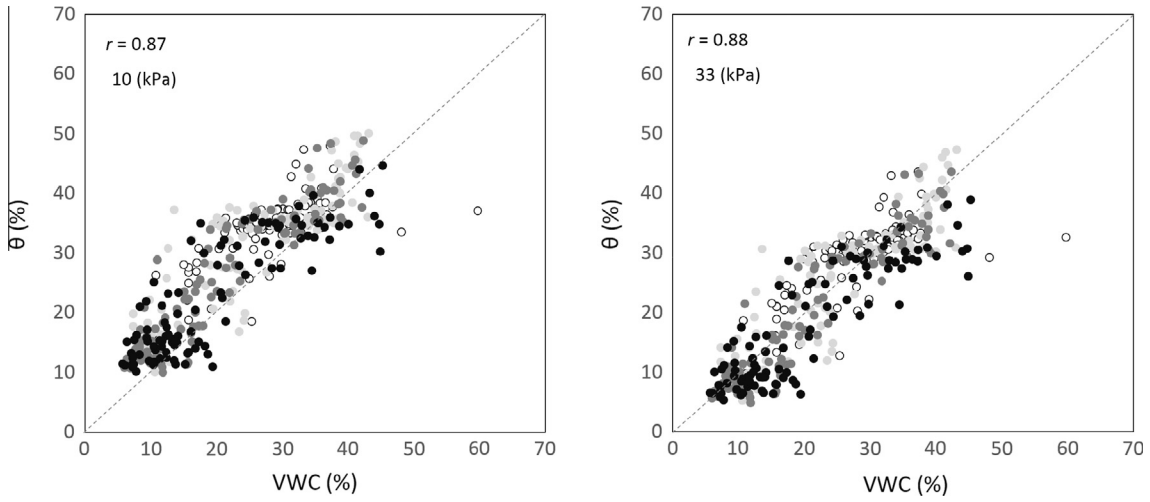

Fig. 7. The relationship of the volumetric water content (% VWC) predicted by pseudo continuous pedotransfer functions (PC-PTF) at −10 kPa and −33 kPa versus water content (θ) at the time of sampling. The increasing shade of the dots represents samples taken at deeper depths.

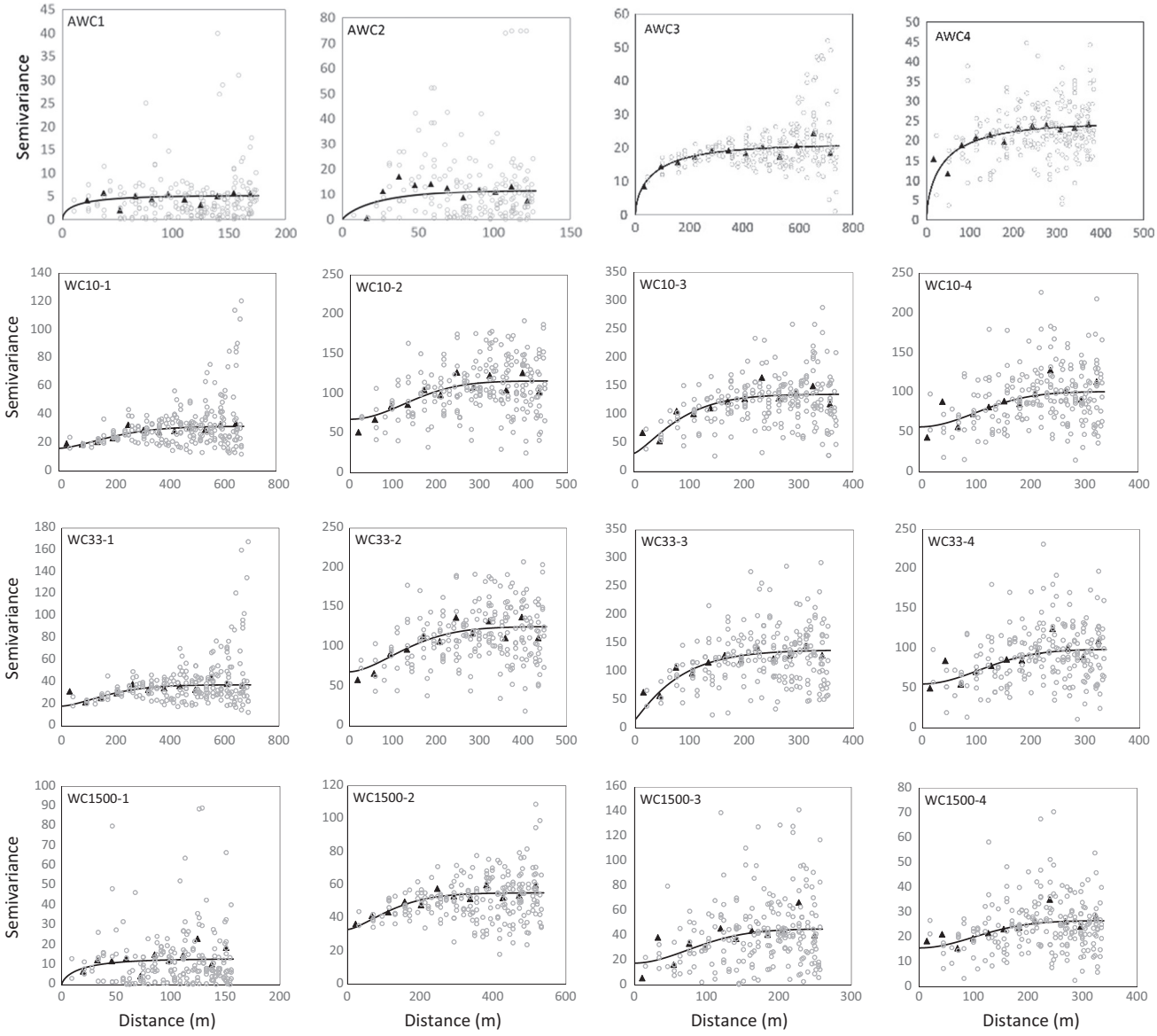

Fig. 8. The semivariograms for water retention data produced from kriging. AWC*x*: available water content at layer *x*; WC*a*-*b*: water content at matric potential *a* (kPa) and layer *b*.

Table 2
The root mean square error (RMSE in $cm^3\ cm^{-3}$) for predicted water content for ten different workflow models at four different depths and three different matric potentials (h (kPa)).

Depth (cm)	h (kPa)	Model									
		1	2	3	4	5	6	7	8	9	10
0–25	−10	0.049	0.050	0.042	0.046	0.041	0.076	0.042	0.042	0.044	0.043
	−33	0.052	0.055	0.044	0.049	0.042	0.071	0.043	0.044	0.045	0.048
	−1500	0.039	0.040	0.029	0.034	0.033	0.055	0.029	0.030	0.030	0.031
25–50	−10	0.098	0.099	0.079	0.091	0.078	0.099	0.081	0.079	0.081	0.084
	−33	0.101	0.103	0.082	0.094	0.084	0.097	0.083	0.082	0.083	0.088
	−1500	0.069	0.070	0.058	0.063	0.058	0.070	0.058	0.058	0.059	0.061
50–75	−10	0.103	0.112	0.085	0.100	0.084	0.092	0.090	0.084	0.095	0.088
	−33	0.102	0.109	0.085	0.099	0.084	0.090	0.088	0.084	0.091	0.088
	−1500	0.059	0.061	0.051	0.059	0.052	0.053	0.051	0.051	0.052	0.053
75–100	−10	0.091	0.096	0.078	0.090	0.075	0.089	0.076	0.075	0.077	0.074
	−33	0.090	0.093	0.077	0.089	0.074	0.087	0.073	0.073	0.074	0.077
	−1500	0.047	0.048	0.040	0.047	0.050	0.059	0.041	0.040	0.041	0.052

Table 3
The mean bias error (MBE, $cm^3\ cm^{-3}$) is used for evaluating the performance of the ten workflow models used to predict water content at four different depths and three different matric potentials (h (kPa)).

Depth (cm)	h (kPa)	Model									
		1	2	3	4	5	6	7	8	9	10
0–25	−10	0.002	0.005	−0.004	0.000	0.000	−0.012	0.004	0.000	−0.003	−0.006
	−33	0.001	0.009	−0.004	0.000	0.001	0.000	0.005	0.000	0.000	0.001
	−1500	0.003	0.009	0.000	0.003	−0.005	0.023	0.005	0.000	0.005	−0.002
25–50	−10	0.005	0.020	0.001	0.007	0.000	−0.013	0.005	0.001	0.005	0.000
	−33	0.004	0.025	0.001	0.009	0.000	0.002	0.008	0.000	0.006	−0.004
	−1500	0.003	0.016	0.000	0.007	−0.001	0.020	0.006	0.000	0.004	−0.002
50–75	−10	0.005	0.039	−0.001	0.019	0.001	0.011	0.019	−0.002	0.024	0.001
	−33	0.005	0.034	−0.001	0.016	0.001	0.012	0.019	−0.002	0.021	0.000
	−1500	0.003	0.012	0.000	0.006	0.009	0.008	0.009	−0.001	0.009	−0.001
75–100	−10	0.000	0.027	−0.004	0.013	0.000	0.016	0.019	0.001	0.012	−0.003
	−33	−0.002	0.019	−0.005	0.008	−0.001	0.017	0.015	0.000	0.009	−0.008
	−1500	−0.001	0.005	−0.002	0.003	0.011	0.012	0.005	0.000	0.000	0.014

7, 5 and 3 (RMSE = 0.063 $cm^3\ cm^{-3}$) showed the highest potential for mapping AWC. On average the MBE values were close to zero indicating that systematic over/under estimation was not an issue.

Fig. 9 shows the maps of AWC predicted for different layers and for the entire effective root zone (i.e. 1 m). The AWC maps of individual layers were produced using the model 8, considering water content at −10 kPa as FC for the entire field. To generate a map for the entire effective root zone, AWC for each sampling location was calculated then interpolated. Finally, the Natural Breaks (Jenks) method was employed to classify the AWC map. In general, there were three regions within the field with low AWC: (i) a region in the southern portion of the field somewhat outside both pivots circles, (ii) a triangular shaped region in the eastern part of the field covering the pivot point of the eastern irrigation system, and (iii) a region in the northwestern part of the field almost covering one-third of the western irrigation system (Fig. 9). The mean AWC was almost the same for the first and second layer but dropped by up to 20% for the third and fourth layer. The standard deviation of the AWC was 0.54%, 2.32%, 3.62% and 3.28% for the layers 1, 2, 3 and 4, respectively. The AWC within the effective root zone varied substantially across the field (min AWC: 5.34%; max: 20.95%; mean = 11.45% and SD = 3.28%) by showing a difference as great as almost fourfold between soil with low and high AWC.

3.3. Soil water retention, yield and EC_a variation

Table 4 summarizes the correlation of EC_a and yield data with water retention at FC and PWP among different layers. Note, that the correlation information was only obtained for cores, hence water retention information was predicted by PC-PTF for cores ($n = 100$ (points) × 4 (depths) = 400) without interpolation. The EC_a showed a moderate correlation, from 0.39 to 0.75, with water retention and AWC. As it was expected, the EC_a-shallow had a greater correlation with water retention at first layer while EC_a-deep indicated a higher correlation with water retention at second, third and fourth layers. On average, there was no difference between the correlations of EC_a with water content at different matric potentials but yield showed higher correlation with water content at FC than with water content at PWP. Both cotton and Soybean had low to moderate correlation with water retention and AWC ranging from 0.35 to 0.65 and from 0.34 to 0.56, respectively. The highest correlation ($r = 0.75$) was observed between AWC in the entire effective root zone (considering water content at −10 kPa as the FC) and EC_a-deep readings. The same was true for yield data such that the highest correlation (0.62 and 0.56 for cotton and soybean, respectively) occurred for AWC within the entire effective root zone. This is because EC_a deep readings integrates the soil over more than one layer and yield is also affected more by the available water within the entire effective root zone in comparison with the water status of individual layers.

4. Discussion

4.1. Model performance analysis

The PC-PTF had an RMSE as low as 0.056 $cm^3\ cm^{-3}$ for the UNSODA data and also showed a high performance ($r = 0.89$ and RMSE = 0.052 $cm^3\ cm^{-3}$) for the study site. Nebel et al. (2010)

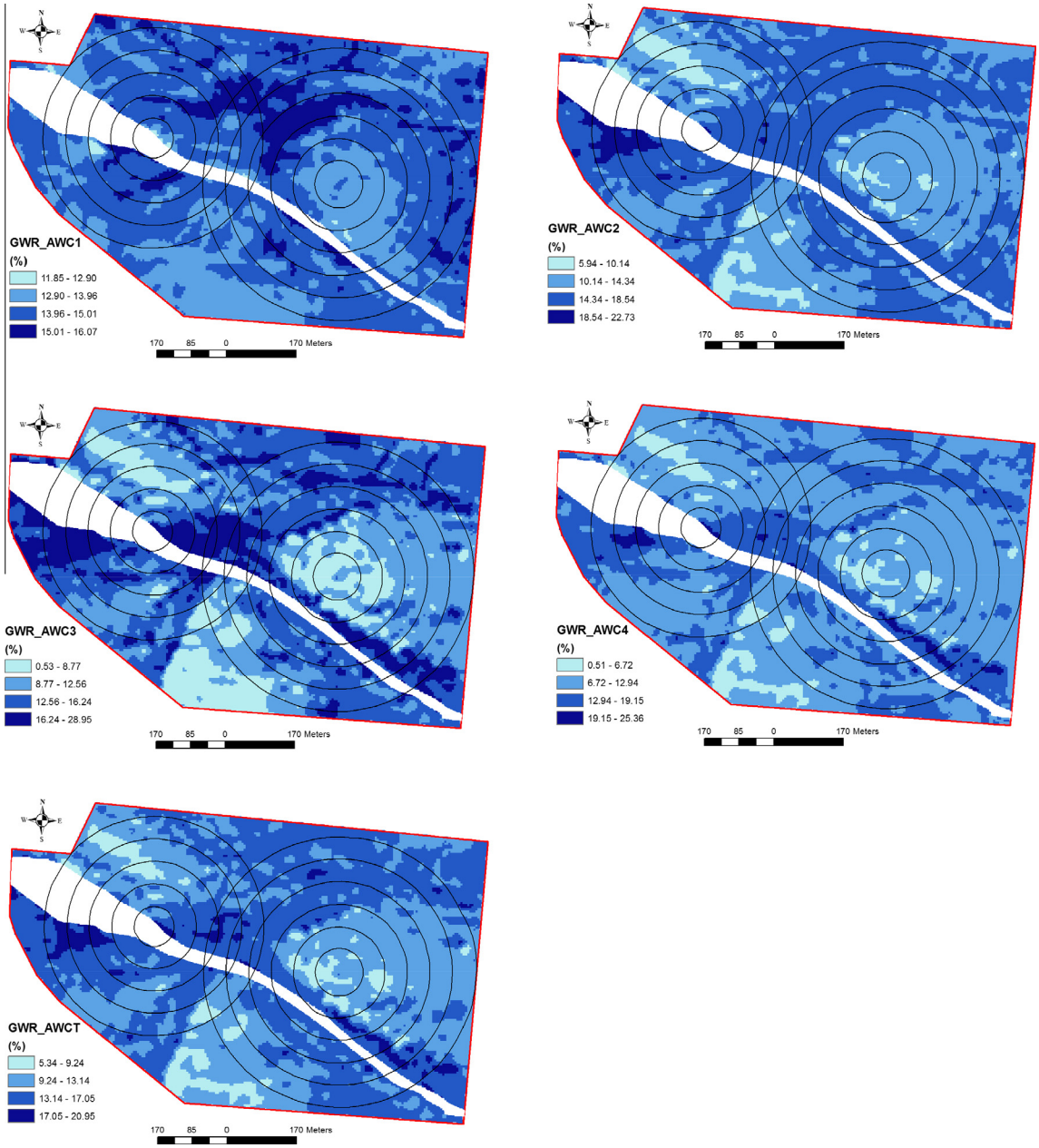

Fig. 9. The model 8 workflow (Fig. 4) used geographically weighted regression (GWR) to produce soil available water content (AWC) maps for the entire effective root zone (AWCT) and at 4 different depths (AWC1 to, AWC4).

evaluated the ability of some published PTFs to explain the spatial variability of water retention at FC and PWP, reporting correlation coefficients from 0.35 to 0.69. Our findings on the accuracy and reliability of the PC-PTFs are comparable to previous studies by Haghverdi et al. (2012, 2014). Haghverdi et al. (2014) reported RMSEs of 0.040 and 0.047 $cm^3\ cm^{-3}$, respectively for their PC-PTF that was applied to two data sets from Belgium and Turkey, respectively. The PC-PTF even showed a better performance, RMSE = 0.028 $cm^3\ cm^{-3}$, on a small data set from Iran (Haghverdi et al., 2012). The variation in PC-PTF performance among studies is related to the characteristics of the data sets. In previous studies, training and test soil samples belonged to small local data sets but we used UNSODA data set that included samples from different regions around the world. Deriving PTFs via large data sets comprising soils from different origins creates higher error than establishing a PTF by a local/regional dataset. For instance, Rosetta PTF and a support vector machine based PTF, when derived and tested on a big dataset, had RMSE equal to 0.053 $cm^3\ cm^{-3}$ and 0.067 $cm^3\ cm^{-3}$, respectively (Twarakavi et al., 2009). Haghverdi et al. (2015a) used the same subset of samples from UNSODA as we did to establish and test the accuracy of a novel non-parametric PTF which predicts the WRC using k nearest neighbor technique and van Genuchten soil hydraulic equation (Van Genuchten, 1980). Their PTF performed very similar (i.e. RMSE = 0.057 $cm^3\ cm^{-3}$) to PC-PTF in our study. In another study, Schaap et al. (2001) reported RMSE equal to 0.068 $cm^3\ cm^{-3}$ for Rosetta PTF established and tested for a large number of soil hydraulic data.

The spatial arrangement of zones with low and high AWC matched our observation during sampling on soil texture and volumetric water content spatial heterogeneity. It suggests a combination of PC-PTF and interpolation as a useful method to produce

Table 4
Correlation coefficients between apparent electrical conductivity (EC_a, mS m^{-1}) and yield data with water content at different depths and three different matric potentials (h (kPa)), predicted by the pseudo continuous pedotransfer function (PC-PTF) for soil samples collected from the field of study (n = 100 (points) × 4 (depths) = 400).

Depth	Matric potential, (kPa)	EC_a – shallow (mS m^{-1})	EC_a – deep (mS m^{-1})	Cotton 2012 (Mg ha^{-1})	Soybean 2009 (Mg ha^{-1})
1st	−10	0.68	0.50	0.35	0.42
	−33	0.72	0.54	0.36	0.44
	−1500	0.75	0.58	0.36	0.45
2nd	−10	0.59	0.67	0.50	0.40
	−33	0.59	0.68	0.50	0.39
	−1500	0.56	0.64	0.44	0.34
3rd	−10	0.45	0.65	0.57	0.42
	−33	0.45	0.65	0.55	0.40
	−1500	0.42	0.61	0.51	0.34
4th	−10	0.39	0.61	0.51	0.46
	−33	0.40	0.62	0.50	0.44
	−1500	0.39	0.59	0.44	0.38
AWCT[a]	(−10) – (−1500)	0.58	0.75	0.64	0.55
AWCT	(−33) – (−1500)	0.52	0.69	0.65	0.56

[a] Available water content throughout the effective root zone.

high resolution maps of soil AWC. The error of the regionalization process comes from both calculation and interpolation steps, yet according to Sinowski et al. (1997) different error components, i.e. PTF and interpolation, may compensate each other. Herbst et al. (2006) used different interpolation techniques to predict some hydraulic properties of soil in a micro-scale catchment and found the error of different methods to be roughly in the same range.

None of the 10 models in our study consistently performed best for all layers and matric potentials. Zhang and Srinivasan (2009) reported an increase in the precipitation spatial prediction accuracy when elevation and spatial coordinate were considered as ancillary data through interpolation process while no interpolation method consistently outperformed other approaches. On the other hand, Eldeiry and Garcia (2010) used remotely sensed images from the Landsat satellite to estimate soil salinity using multiple techniques. They found that ordinary kriging performed better than regression kriging and co-kriging. They found higher autocorrelation among soil salinity data compared to cross-correlation between salinity and remotely sensed data that is a potential reason for the better results from ordinary kriging. There was a considerable spatial agreement between EC_a data and soil water content in our study. We collected the EC_a data before the other data sets when the study area was believed to be close to its field capacity. Consequently, EC_a provided useful information on spatial heterogeneity of soil water retention throughout the study area. This result confirmed the efficiency of EC_a as a proxy for AWC in our study and also in turn explains the better performance of the GWR, co-kriging and regression kriging models, over the ordinary kriging models. We observed up to 19% improvement due to incorporating EC_a data in our models which was in agreement with the reported result by Herbst et al. (2006) who observed up to 15% improvement by considering terrain attributes as ancillary data in the spatial prediction process. Regression kriging used the quality information provided by EC_a in the form of maps of covariates to explain part of the variation in soil water content. In GWR multiple linear regression fits provided local estimation of regression coefficients that helped explain the influence of EC_a on soil water content. Harris et al. (2010) compared the performance of different interpolation techniques using simulated date with different levels of spatial autocorrelation and heterogeneity. They reported better results for models that account for spatial autocorrelation as well as spatially varying relationships (i.e. universal kriging model specified with local neighborhoods and geographically weighted regression kriging). Further investigation is needed to evaluate the performance of novel hybrid interpolation techniques to predict soil water content at field-level.

In general, CI (i.e. calculation–interpolation) was a more accurate procedure than IC (i.e. interpolation–calculation) in this study. This is because for the former, soil water content was the only variable interpolated, while for the latter each input variable had to be interpolated. This increased the error in a model's workflow (Bechini et al., 2003), especially when one or some of the variables do not show spatial structure or spatial autocorrelation. Moreover, some inconsistencies with the spatial prediction of single fractions of the particle size distribution may have occurred (Herbst et al., 2006). In the study site, a weak spatial dependency was observed for BD. Since BD was an input to the PC-PTF, the error associated with interpolated BD likely contributed to the higher error of the IC procedure. However, CI may not be as efficient as IC if a continuous realization of WRC over a wide range of matric potentials is needed. Saito et al. (2009) compared some fitting-interpolation scenarios in order to get a spatial interpolation of WRC. They reported lower prediction error for interpolation-fitting methods. According to Heuvelink and Pebesma (1999), if you use the CI approach, the interpolation step will not fully utilize the available information on the spatial structure of inputs. Therefore, if many inputs are available with different spatial structures, IC might be a more accurate option.

4.2. Practical challenges and findings

The sampling density and scheme will affect the error associated with the spatial prediction process (Herbst et al., 2006). Sampling is time-consuming and expensive, consequently, it is desired to minimize sampling density. Given the promising results achieved by incorporating EC_a data in the spatial modeling process along with the high degree of spatial agreement observed between EC_a and soil physical data, it may be feasible to reduce the need for more difficult data collection (such as soil texture and BD) through sampling while maintaining the target level of accuracy. Debaene et al. (2014) studied the relationship between density of samples and prediction of several soil properties at the farm-scale using visible and near infrared spectroscopy methods. They showed that 1.5 samples ha^{-1} is adequate to predict soil organic matter content and texture. Our sampling density of 1.42 samples ha^{-1} was close to their recommendation. Taking 1 samples ha^{-1} is usually considered the greatest sampling density that a farmer can afford (Kerry et al., 2010). However, the additional weight of variable rate irrigation management is to collect samples at deeper depths to

adequately cover the effective crop root zone. Analyzing the effect of the density of collected soil samples on the performance of the spatial modeling techniques is out of the scope of this study. Iqbal et al. (2005) recommended sampling intervals of <100-m in order to detect boundaries of soil hydraulic properties in an alluvial floodplain soil in the region of the Mississippi Delta. Further investigation is needed to determine the tradeoffs between the optimum number of samples, practical limitations, and knowledge of the soil variability.

The spatial distribution of soil texture in the field of study was the primary factor influencing AWC at different depths. We found that a reduction in AWC with increasing depth was consistent with an increase in sand percentage with depth. Moreover, a strong positional similarity was observed among the AWC maps. In the same manner, Iqbal et al. (2005) found a similar match between the spatial distribution of soil hydraulic properties with clay and sand composition. EC_a showed good correlation with soil physical properties and soil hydraulic properties in the field of study. EC_a was also a very useful proxy for mapping AWC, i.e., the accuracy of soil water content maps improved when EC_a was incorporated in the workflow models. Abdu et al. (2008) showed that EC_a was a useful proxy for mapping the heterogeneity of a watershed's soil texture. Using proxies such as EC_a is extremely practical in helping to minimize the number of samples collected and in turn reducing the associated cost of the mapping process.

Spatial variation in soil AWC was strong with up to a fourfold increase in both fine- and coarse-textured soils within the study area. This spatial variability of AWC with soil texture had a moderate influence on yield. Using a multi-year study with surface drip irrigation system, Duncan (2012) showed that optimized supplemental irrigation management of cotton is not identical across soils with low and high AWCs. Currently, most farmers use a uniform irrigation application rate regardless of the spatial heterogeneity of soils within their fields. At worst, this management causes partial over or under irrigation, depending on the soil texture, and consequently yield reduction. Over irrigation in soils with high AWC causes cotton to increase its vegetative growth and decrease its yield. On the other hand, severe deficit irrigation in soils with lower AWC decreases the yield by influencing the boll number and retention (Gwathmey et al., 2011). AWC maps at high spatial resolution could be used to delineate irrigation management zones for variable rate irrigation. Given the observed variation of AWC with depth, the spatial arrangement of management zones may even vary throughout the growing season as roots penetrate into deeper layers. Therefore, a temporally dynamic zoning system may be needed to fulfill crop water requirements (Haghverdi et al., 2015b). The available center pivots in this study site like other similar systems are capable of varying irrigation rates across a field by changing their travel speed. Developing a variable rate irrigation strategy for this field is expected to increase the yield as well as water use efficiency. This, in turn, would reduce other potential problems including leaching, runoff and erosion. Further studies are needed to precisely investigate different irrigation management strategies and to economically compare the profitability of variable rate systems as opposed to an optimized management system that uses available pivots with limited ability to control speed.

5. Conclusion

The maps of the spatial heterogeneity of AWC within the effective root zone could be used for irrigation zone delineation and variable rate irrigation scheduling. There are many techniques and protocols in the literature that provide non-spatial point estimation of soil water retention. However, this literature is limited in regards to the production of high-resolution maps of soil hydraulic properties. PC-PTF performed well for predicting AWC of soils with different textures. Additionally, we found that the incorporation of EC_a data into our workflow models was beneficial for interpolation of point predictions of AWC, with the best performance resulting when it was used as an input predictor in GWR models. However, a firm understanding of soil characteristics that affect soil EC_a is needed for each site prior to applying EC_a in an appropriate workflow modeling, a suggestion that we leave for future investigations. We showed that the spatial heterogeneity of soil hydraulic attributes could affect yield distribution. Consequently, site-specific spatial models are required to investigate the optimum application of irrigation in the presence of field-level heterogeneity of soil hydraulic properties. The resulting map predictions can then be used as an input for developing effective variable rate irrigation management scenarios.

References

Abdu, H., Robinson, D.A., Seyfried, M., Jones, S.B., 2008. Geophysical imaging of watershed subsurface patterns and prediction of soil texture and water holding capacity. Water Resour. Res. 44 (4).

Archie, G.E., 1942. The electrical resistivity log as an aid in determining some reservoir characteristics. Trans. Am. Inst. Min. Metall. Eng. 146, 54–61.

Bechini, L., Bocchi, S., Maggiore, T., 2003. Spatial interpolation of soil physical properties for irrigation planning. A simulation study in northern Italy. Eur. J. Agron. 19 (1), 1–14.

Bouma, J., 1989. Using soil survey data for quantitative land evaluation. Adv. Soil Sci. 9, 177–213.

Corwin, D.L., Lesch, S.M., 2005. Apparent soil electrical conductivity measurements in agriculture. Comput. Electron. Agric. 46 (1), 11–43.

Debaene, G., Niedźwiecki, J., Pecio, A., Żurek, A., 2014. Effect of the number of calibration samples on the prediction of several soil properties at the farm-scale. Geoderma 214, 114–125.

Demuth, H., Beale, M., 2000. Neural Network Toolbox. Mathworks Inc.

Duncan, H.A., 2012. Locating the Variability of Soil Water Holding Capacity and Understanding its Effects on Deficit Irrigation and Cotton Lint Yield. Master's Thesis, University of Tennessee. <http://trace.tennessee.edu/utk_gradthes/1286>.

Efron, B., Tibshirani, R.J., 1993. An Introduction to the Bootstrap. Monographs on Statistics and Applied Probability. Chapman and Hall, New York.

Eldeiry, A.A., Garcia, L.A., 2010. Comparison of ordinary kriging, regression kriging, and cokriging techniques to estimate soil salinity using LANDSAT images. J. Irrig. Drain. Eng. 136 (6), 355–364.

Fotheringham, A.S., Brunsdon, C., Charlton, M., 2002. Geographically Weighted Regression: The Analysis of Spatially Varying Relationships. John Wiley & Sons (269 p).

Ferrer Julià, M., Estrela Monreal, T., del Corral, Sánchez., Jiménez, A., García Meléndez, E., 2004. Constructing a saturated hydraulic conductivity map of Spain using pedotransfer functions and spatial prediction. Geoderma 123 (3), 257–277.

Goovaerts, P., Kerry, R., 2010. Using ancillary data to improve prediction of soil and crop attributes in precision agriculture. In: Geostatistical Applications for Precision Agriculture. Springer, Netherlands, pp. 167–194.

Gwathmey, C.O., Leib, B.G., Main, C.L., 2011. Lint yield and crop maturity responses to irrigation in a short-season environment. J. Cotton Sci. 15, 1–10.

Haghverdi, A., Cornelis, W.M., Ghahraman, B., 2012. A pseudo-continuous neural network approach for developing water retention pedotransfer functions with limited data. J. Hydrol. 442, 46–54.

Haghverdi, A., Öztürk, H.S., Cornelis, W.M., 2014. Revisiting the pseudo continuous pedotransfer function concept: impact of data quality and data mining method. Geoderma 226, 31–38.

Haghverdi, A., Leib, B.G., Cornelis, W.M., 2015a. A simple nearest-neighbor technique to predict the soil water retention curve. Trans. ASABE 58 (3).

Haghverdi, A., Leib, B.G., Washington-Allen, R.A., Ayers, P.D., Buschermohle, M.J., 2015b. Perspectives on delineating management zones for variable rate irrigation. Comput. Electron. Agric. 117, 154–167.

Harris, P., Fotheringham, A.S., Crespo, R., Charlton, M., 2010. The use of geographically weighted regression for spatial prediction: an evaluation of models using simulated data sets. Math. Geosci. 42 (6), 657–680.

Hedley, C.B., Yule, I.J., 2009a. A method for spatial prediction of daily soil water status for precise irrigation scheduling. Agric. Water Manag. 96 (12), 1737–1745.

Hedley, C.B., Yule, I.J., 2009b. Soil water status mapping and two variable-rate irrigation scenarios. Precis. Agric. 10 (4), 342–355.

Hedley, C.B., Roudier, P., Yule, I.J., Ekanayake, J., Bradbury, S., 2013. Soil water status and water table depth modelling using electromagnetic surveys for precision irrigation scheduling. Geoderma 199, 22–29.

Hengl, T., Heuvelink, G.B., Rossiter, D.G., 2007. About regression-kriging: from equations to case studies. Comput. Geosci. 33 (10), 1301–1315.

Herbst, M., Diekkrüger, B., Vereecken, H., 2006. Geostatistical co-regionalization of soil hydraulic properties in a micro-scale catchment using terrain attributes. Geoderma 132 (1), 206–221.
Heuvelink, G.B., Pebesma, E.J., 1999. Spatial aggregation and soil process modelling. Geoderma 89 (1), 47–65.
Iqbal, J., Thomasson, J.A., Jenkins, J.N., Owens, P.R., Whisler, F.D., 2005. Spatial variability analysis of soil physical properties of alluvial soils. Soil Sci. Soc. Am. J. 69 (4), 1338–1350.
Jana, R.B., Mohanty, B.P., 2011. Enhancing PTFs with remotely sensed data for multi-scale soil water retention estimation. J. Hydrol. 399 (3), 201–211.
Kerry, R., Oliver, M.A., Frogbrook, Z.L., 2010. Sampling in precision agriculture. In: Geostatistical Applications for Precision Agriculture. Springer, Netherlands, pp. 35–63.
Li, J., Heap, A.D., Potter, A., Daniell, J.J., 2011. Application of machine learning methods to spatial interpolation of environmental variables. Environ. Model. Softw. 26 (12), 1647–1659.
Nebel, Á.L.C., Timm, L.C., Cornelis, W., Gabriels, D., Reichardt, K., Aquino, L.S., Pauletto, E.A., Reinert, D.J., 2010. Pedotransfer functions related to spatial variability of water retention attributes for lowland soils. Rev. Bras. Ciência Solo 34 (3), 669–680.
Nemes, A., Schaap, M.G., Leij, F.J., Wösten, J.H.M., 2001. Description of the unsaturated soil hydraulic database UNSODA version 2.0. J. Hydrol. 251 (3), 151–162.
Oliver, M.A., 2010. An overview of geostatistics and precision agriculture. In: Geostatistical Applications for Precision Agriculture. Springer, Netherlands, pp. 1–34.
Rivers, E.D., Shipp, R.F., 1972. Available water capacity of sandy and gravelly North Dakota soil. Soil Sci. 113, 74–80.
Romano, N., Santini, A., 2002. Field. In: Dane, J.H., Topp, G.C. (Eds.), Methods of Soil Analysis. Part 4, Physical Methods, Soil Sci. Soc. Am. Book Ser., vol. 5. Soil Sci. Soc. of Am., Madison, Wis., pp. 721–738.
Saey, T., Van Meirvenne, M., Vermeersch, H., Ameloot, N., Cockx, L., 2009. A pedotransfer function to evaluate the soil profile textural heterogeneity using proximally sensed apparent electrical conductivity. Geoderma 150 (3), 389–395.
Saito, H., Seki, K., Šimůnek, J., 2009. An alternative deterministic method for the spatial interpolation of water retention parameters. Hydrol. Earth Syst. Sci. 13 (4), 453–465.
Schaap, M.G., Leij, F.J., van Genuchten, M.Th., 2001. ROSETTA: a computer program for estimating soil hydraulic parameters with hierarchical pedotransfer functions. J. Hydrol. 251, 163–176.
Sharma, V., Kilic, A., Kabenge, I., Irmak, S., 2011. Application of GIS and geographically weighted regression to evaluate the spatial non-stationarity relationships between precipitation vs. irrigated and rainfed maize and soybean yields. Trans. ASABE 54 (3), 953–972.
Sinowski, W., Scheinost, A.C., Auerswald, K., 1997. Regionalization of soil water retention curves in a highly variable soilscape, II. Comparison of regionalization procedures using a pedotransfer function. Geoderma 78 (3), 145–159.
Sudduth, K.A., Kitchen, N.R., Wiebold, W.J., Batchelor, W.D., Bollero, G.A., Bullock, D. G., Clay, D.E., Palm, H.L., Pierce, F.J., Schuler, R.T., Thelen, K.D., 2005. Relating apparent electrical conductivity to soil properties across the north-central USA. Comput. Electron. Agric. 46 (1), 263–283.
Twarakavi, N.K., Šimůnek, J., Schaap, M.G., 2009. Development of pedotransfer functions for estimation of soil hydraulic parameters using support vector machines. Soil Sci. Soc. Am. J. 73 (5), 1443–1452.
Van Genuchten, M.Th., 1980. A closed-form equation for predicting the hydraulic conductivity of unsaturated. Soil Sci. Soc. Am. J. 43, 892–898.
Vereecken, H., Weynants, M., Javaux, M., Pachepsky, Y., Schaap, M.G., van Genuchten, M.Th., 2010. Using pedotransfer functions to estimate the van Genuchten-Mualem soil hydraulic properties: a review. Vadose Zone J. 9 (4), 795–820.
Wösten, J.H.M., Pachepsky, Y.A., Rawls, W.J., 2001. Pedotransfer functions: bridging the gap between available basic soil data and missing soil hydraulic characteristics. J. Hydrol. 251, 123–150.
Zhang, X., Srinivasan, R., 2009. GIS-Based spatial precipitation estimation: a comparison of geostatistical approaches. Am. Water Resour. Assoc. 45 (4), 894–906.